Mechanical Strength of the Titin Z1Z2/Telethonin Complex

Eric H. Lee[§], Mu Gao[¶], Nikos Pinotsis[†],Matthias Wilmanns[†], Klaus Schulten[¶*]

October 26, 2005

[§] Center for Biophysics and Computational Biology and Beckman Institute, University of Illinois at Urbana-Champaign, Urbana, USA
[¶] Department of Physics and Beckman Institute, University of Illinois at Urbana-Champaign, Urbana, USA
[†] EMBL-Hamburg Outstation, DESY, Hamburg, Germany

[*] To whom correspondence should be addressed. Email: kschulte@ks.uiuc.edu. Phone: 217-244-1604. Fax: 217-244-6078.

Summary

The giant protein titin provides muscle upon its extension with a passive restoring force and is essential for maintaining the integrity of the muscular sarcomere. In order for titin to reversibly stretch and contract, its two ends, the terminal domains, must be anchored at the sarcomeric Z-disc and M-line. Here we investigate the role that telethonin, a protein which joins the ends of two titin molecules together at the Z-disc, plays in anchoring titin to one end of the sarcomere. Using molecular dynamics (MD) simulations, we have explored the mechanical strength of the structurally resolved titin Z1Z2-telethonin complex, namely, its ability to bear strong forces such as those that titin encounters during passive muscle stretch. Our results show that not only does this complex resist high levels of mechanical force, suggesting that telethonin is a major component of the N-terminal titin anchor, but also that telethonin acts to distribute these forces between its two joined titin Z2 domains to protect the most proximal Z1 domain from bearing too much stress. Our simulations also reveal that in the absence of telethonin, apo-titin Z1Z2 exhibits significantly decreased resistance to mechanical stress, and that the N-terminal segment of telethonin (residues 1-89) does not exhibit a stable fold conformation when it is unbound from titin Z1Z2. Consequently, our study sheds light on a key but little studied architectural feature of biological cells, the existence of strong mechanical links that glue separate proteins together.

Introduction

One of the most important properties of striated muscle is its elasticity. In fact, muscle fibers can achieve greater than two-fold extension with no significant loss of structural integrity. During extension, the muscle sarcomere develops a restoring force to bring the muscle fiber back to equilibrium length, at the same time preventing the thin actin filaments from sliding outside the zone of the thick myosin filaments. The giant muscle protein titin, spanning one-half of the sarcomere and nearly 1 μm in length with a molecular weight of up to 4 MDa, plays a significant role in maintaining sarcomere integrity by generating this passive restoring force (Wang, 1996; Erickson, 1997; Maruyama, 1997; Linke, 2000; Tskhovrebova and Trinick, 2003; Granzier and Labeit, 2004). Titin is composed of ∼300 tandem repeats of mainly immunoglobulin-like (Ig) and fibronectin type III (FnIII) domains, as well as a few unique domains. The N-terminal section of titin originates from the sarcomeric Z-disc (Gautel et al., 1996; Mues et al., 1998; Pyle and Solaro, 2004) and its C-terminal region is an integral component of the sarcomeric M-line (Furst et al., 1988; Obermann et al., 1997).

In addition to providing extension, recent studies suggest that the terminal regions of titin serve in part as sensor complexes that respond to passive stretch force (Miller et al., 2004). In the C-terminal region, mechanical force can induce an activated conformation of the titin kinase domain (Gräter et al., 2005; Lange et al., 2005). At the very N-terminal region of titin, a sensor complex is formed based on two titin Ig domains, Z1 and Z2 (Knöll et al., 2002). The core part of this complex relies on the anchoring of Z1 and Z2 through the ligand telethonin (Valle et al., 1997; Gregorio et al., 1998; Faulkner et al., 2001). Telethonin is one of the most abundant transcripts in striated muscle. Binding studies have revealed that it is highly specific for both titin Z1 and Z2, but not for Z1 or Z2 individually (Faulkner et al., 2001). Biochemical studies of telethonin have shown that its presence, in conjunction with titin Z1Z2, is required for progression of muscle growth (Gregorio et al., 1998). Point mutations to telethonin resulting in premature stop codons have been correlated to a form of limb girdle muscular dystrophy (type 2A) (Schroder et al., 2001; Itoh-Satoh et al., 2002; Vainzof et al., 2002; Bonnemann and Laing, 2004; Laval and Bushby, 2004), suggesting that telethonin plays a major role in the stabilization of N-terminal titin at the Z-disc. A variety of Z-disc proteins have been found to interact strongly with telethonin. These include the stretch receptor candidate muscle LIM protein (MLP) (Knöll et al., 2002; Miller et al., 2004), the potassium channel regulation protein minK (Furukawa et al., 2001; Granzier and Labeit, 2004), the muscle growth factor myostatin (Nicholas et al., 2002), and muscle ankyrin repeat proteins sAnk1 and Ankrd2 (Kontrogianni-Konstantopoulos and Bloch, 2003; Kojic et al., 2004). The vital roles each of these proteins play and their binding to telethonin further corroborates the idea that the telethonin-Z1Z2 complex serves as a platform for engaging stress sensoring proteins.

Very recently, a crystal structure of the N-terminal half of telethonin in complex with titin Z1 and Z2 has been reported (Zou et al., 2005). Unlike typical ligand-binding through insertion of the ligand into a binding pocket of the receptor, in

this crystal structure the receptor Z1Z2 domains of two antiparallel titin N-termini (named ZA and ZB) are surprisingly joined together by an N-terminal fragment of the ligand telethonin (TLT) through β-strand cross-linking (see Fig. 1), a structural motif that also appears in pathological fibril formation (Tjernberg et al., 1999; Walsh et al., 2001; Karanicolas and Brooks, 2003; Wang et al., 2005a). We denote this $(Z1Z2)_2$-telethonin complex as the T_2T complex. On the other hand, it is known that β-strands can form mechanically stable β-sheets that resist stress in so-called *mechanical proteins*, such as titin Ig domains or fibronectin type III like modules (Rief et al., 1997; Lu et al., 1998; Marszalek et al., 1999; Lu and Schulten, 1999; Gao et al., 2003; Craig et al., 2004). Naturally this raises the question: Does the β-strand cross-linking between titin and telethonin represent a novel ligand-binding strategy that provides a mechanically stable linkage?

Using molecular dynamics (MD) simulations (Isralewitz et al., 2001), we have studied the mechanical design of the T_2T complex and its individual components by probing their mechanical responses. We first compared the stability of the T_2T complex with that of an apo-Z1Z2 structure through constant velocity SMD simulations. To reveal the key force-bearing elements for each case, we carried out constant force simulations and analyzed the structural changes corresponding to main events that lead to complex unbinding or protein unfolding. Lastly, we examined the stability of isolated telethonin fragment alone. We found that the binding of telethonin stabilizes both itself and Z1Z2 through the β-strand cross-linking at the binding interface.

Results

The following section is based on the simulations summarized in Table 1. Please refer to the Experimental Procedures section for details on simulation system setup and parameters.

Titin Z1Z2-telethonin (T_2T) complex equilibration and stability. Equilibration of the solvated titin Z1Z2-telethonin (T_2T) complex (simA) for 1 ns revealed a stable conformation with an RMSD value of 1.75 Å relative to the crystal structure. The latter structure contains only the N-terminal segment of telethonin (residues 1 to 89) in contact with titin Z1Z2, which is the relevant region of telethonin for investigating its role for joining two titin chains. An illustration of the equilibrated T_2T complex, a schematic of the β-strand alignment, and a view of the extensive surface contacts between the titin and the telethonin fragment is shown in Fig 1. During the equilibration, all backbone hydrogen bonds are stably formed at the binding interface between the G β-strands (G_{Z1_A}, G_{Z1_B}, G_{Z2_A}, G_{Z2_B}) of the four titin Ig domains ($Z1_A$, $Z2_A$, $Z1_B$, $Z2_B$) and the ABCD β-strands of telethonin (A_{TLT}, B_{TLT}, C_{TLT}, D_{TLT}).

It has been suggested that telethonin plays a major role in anchoring the proximal end of titin to the sarcomeric Z-disc (Gregorio et al., 1998). Such a titin anchor must be able to bear a mechanical force load without significant unfolding or distortion. The crystal structure of the T_2T complex revealed a strong receptor-ligand interface dominated by β-strand cross-linking. To investigate the effect of this cross-link interface on the mechanical stability of the Z1Z2 domains, we conducted a constant velocity SMD simulation (simA2) to stretch the T_2T complex. For this purpose, a harmonic spring was attached to one C-terminal titin Z2 C_α atom, while the opposing terminal C_α atom was fixed (see Fig. 2A) on the opposing strand of the complex. At a pulling velocity of 0.05 Å/ps over 1 ns the complex became unbound; the unbinding of the complex was accompanied by a pronounced force peak of 1900 pN (Fig. 2).

This peak force coincides with the detachment of one titin Z2 domain ($Z2_A$) from the telethonin fragment (Fig. 2B), rather than with the unfolding of one of the Z2 domains seen in stretching simulations of apo-Z1Z2 (see below). The detachment of $Z2_A$ started with the separation of β-strand G_{Z2_A} from β-strand D_{TLT}. As stretching continues, the A-strand of the detached Z2 domain starts unraveling to provide further extension while the Ig-domain unfolds.

Z1Z2-telethonin β-strand cross-linking mechanically stabilizes the complex. Although constant velocity simulations are useful for probing mechanical stability and reproducing force-extension profiles for comparison with, for example, AFM experiments, the unfolding in constant velocity MD simulations is often too fast to reveal details behind the key unbinding events. To further characterize the mechanical stability and unfolding barrier of the T_2T complex, we performed constant force SMD simulations (simB1-4) where the magnitude of the applied force is chosen low enough so that the complex is "stuck" in front of the unbinding barrier for at least

a few hundred picoseconds. A constant force of the same magnitude was applied to the C-termini of the two titin Z2 domains along opposite directions roughly parallel to the β-strand cross-linking interface (see Fig. 3A); this direction is likely closest to the one along which the actual titin T_2T complex experiences forces during muscle stretch where the tension would originate further down (in the distal direction) the sarcomere.

SimB1-simB4 were conducted using stretching forces of 750 pN, 1000 pN, 1200 pN, and 1500 pN, respectively. Figure 3 shows the extension *vs.* time profiles and representative snapshots of the complex from the 1200pN simulation (simB3). In contrast to the unfolding of Z2 observed in the 750 pN constant force stretching simulation of the apo structure (see below), forces of 750 pN and 1000 pN were insufficient to detach either titin Z2 terminus from the telethonin core within 2 ns (only the first ns is shown in Fig. 3). Only forces of 1200 pN and 1500 pN result in detachment of both titin Z2 domains in sequential order (first $Z2_A$, then $Z2_B$) and in a subsequent unraveling of both Z2 Ig-domain β-sheets. The sequence of unbinding events is similar to that observed in the constant velocity simulation (simA2) of the T_2T complex. After an initial 11 Å extension due to alignment of the complex with the force vector and stretching of the termini, the end-to-end distance of the complex fluctuates between 138 and 142 Å, waiting to overcome the unbinding barrier. The crossing of this barrier requires disruption of the cross-links between β-strands D_{TLT} and G_{Z2_A}, as shown in Fig. 3B. The binding interactions subsequently weaken as the $Z2_A$ domain detaches from telethonin. The complex extends slowly along a shoulder in the extension-time curve between 490 ps and 700 ps. During this period, β-strand A_{Z2_A} separates from β-strand B_{Z2_A} as $Z2_A$ begins to unfold (Fig. 3C). Concurrently, a second cross-linked β-strand pair between telethonin and the opposing $Z2_B$ domain, B_{TLT} and G_{Z2_B}, ruptures in a gradual manner through the sequential unzipping of hydrogen bonds (Fig. 3C and D). The two disruptions destabilize the complex, which then unravels rapidly by unfolding of the detached Z2 domains.

Analysis of the interstrand hydrogen bonds between β-strands B_{TLT} and G_{Z2_A} reveals a fascinating dynamic picture of the main unbinding process of the T_2T complex. Figure 4 shows representative snapshots of the hydrogen bond network between strands B_{TLT} and G_{Z2_A} from the 1200pN SMD simulation (simB3). Seven stabilized interstrand hydrogen bonds are initially formed between residues Thr50, His52, Gln54, and Gln56 of B_{TLT} and Thr188, Thr186, Arg184 and Val182 of G_{Z2_A} (see Fig. 4A). At 438 ps, these seven hydrogen bonds concurrently rupture, coinciding with a surge in the interaction energy between the two strands from -43 kcal/mol to -16 kcal/mol (Fig. 4B, plot). Interestingly, three of the broken hydrogen bonds reformed at 469 ps, resulting in a temporary strengthening of the B_{TLT}-G_{Z2_A} interaction energy to -37 kcal/mol (Fig. 4C). When all B_{TLT}-G_{Z2_A} interstrand hydrogen bonds have been broken at 526 ps (Fig. 4D), the protein has already crossed the transition state.

We also performed an additional set of control simulations that applied constant

stretching forces of 750 and 1200 pN (simB5-simB6) using the same fixed and pulled atom setup as simA2. The results of single fixed terminal simulations, simB5-simB6, were similar to those of simB1-simB4 where force was applied to both ends of the protein.

The titin Z1Z2 dimer exhibits a stable apo-structure. While our simulations above reveal details regarding the mechanical stability of the T_2T complex, they do not permit us to judge the stability of its individual components (Z1Z2 and telethonin). In order to determine if titin Z1 and Z2 exhibit a stable conformation when unbound from telethonin, we isolated the Z1Z2 segment ZA ($Z1Z2_A$) from the structure of the complex and equilibrated the segment in an explicit solvent box for 27.8 ns (simC1). As shown in Fig. 5, the backbone RMSD over the entire trajectory for the individual titin Z1 and Z2 modules reveal that each maintained virtually the same structure as in the telethonin-bound form with RMSD values of only 2 Å, whereas the RMSD for the combined titin Z1Z2 segment showed greater deviation from crystal coordinates because the linker region (residues 99 to 101) joining titin Z1 and Z2 was flexible and permitted the two modules to shift relative to each other, from an extended form to a slightly bent form. The angle spanned by two vectors connecting the two terminal C_α atoms to the C_α of linker residue 100 decreased from an initial 157° to 137° at the end of the simulation, which is consistent with the crystallographic observation that apo-Z1Z2 exhibits both extended and bent forms (Olga Mayans, personal communication).

Apo-Z1Z2 unfolds in two major steps. We next examined the mechanical response of Z1Z2 in the absence of telethonin, using the equilibrated apo-$Z1Z2_A$ dimer structure from simC2. In the constant velocity SMD simulation simC3, the N-terminal C_α of $Z1_A$ was fixed while the opposing C-terminal C_α of $Z2_A$ was attached to a harmonic spring pulled at a rate of 0.05 Å/ps for 1.0 ns (see Fig. 2E). Analysis of this trajectory revealed a force peak of 1000 pN accompanying the extension of Z1Z2 (Fig. 2, plot). Notably, this peak force is about half the force required to unbind Z2 from telethonin in the T_2T complex at the same pulling velocity (simA2), suggesting that binding to telethonin confers considerable strength to Z1Z2.

The unfolding pathway of Z1Z2 observed in simC3 is similar to the unfolding pathway seen in published simulations of titin I-band Ig domains I1 and I27 (Lu and Schulten, 2000; Gao et al., 2002b,c). Corresponding to the peak force, the major unfolding event occurs when the interactions between β-strands A_{Z2_A} and B_{Z2_A} and between A'_{Z2_A} and G_{Z2_A} become disrupted, while Z1 remained virtually intact with the exception of minor unfolding of its A'_{Z1_A} strand (Fig. 2F, G).

To further characterize the mechanical stability of titin Z1 and Z2 Ig domains, we performed constant force SMD simulations (simC4) to stretch the terminal ends of the $Z1Z2_A$ dimer with a force of 750 pN. As shown in Figs. 6 and 7, each Z1 or Z2 domain unfolds in two major steps, corresponding to the rupture of two sets of

backbone hydrogen bonds located near its two termini: one set between the A- and the B-strands, and the other between the A' and the G-strands. Upon the application of a stretching force, the flexible terminal and the linker loops were quickly straightened within 15 ps, increasing the end-to-end distance from 102 Å to 119 Å. The two domains reoriented such that the force-bearing components, namely the AB and A'G β-strands, became aligned parallel to the external force. Resistance to unfolding slowed down the elongation of the peptide, proceeding along a plateau-like curve in the end-to-end distance versus time profile. During this period, the extension of the protein increased by about 20 Å, and a series of key unfolding events occurred. The first unfolding event (Fig. 6B) corresponds to disruption of the four hydrogen bonds formed between the two Z1 β-strands A and B at 120 ps. Rupture of these hydrogen bonds leads to the separation of β-strands A and B, causing the interaction energy between the β-strand pair to change from -21 kcal/mol to -12 kcal/mol (Fig 7A, plot). This event was followed by the breaking of a hydrogen bond set between strands A and B of Z2 at 200 ps (Fig. 6C), leading to a jump of the interaction energy between the strands from -34 kcal/mol to -17 kcal/mol (Fig 7B, plot). The unraveling of the two A-strands (one from Z1 and one from Z2) permitted an extension of $\sim$9 Å. Further elongation required disrupting the second force-bearing set of hydrogen bonds formed between the β-strands A' and G. Four A'-G hydrogen bonds of Z1 rupture at 380 ps (Fig. 6D), initiating a rapid unfolding process with significantly decreased resistance as the remaining intact hydrogen bonds of Z1 are broken in an unzipping-like fashion, i.e., one hydrogen bond at a time. During the rapid unfolding of the Z1 domain, the Z2 domain also became partially unfolded after its five interstrand A'-G hydrogen bonds were ruptured at 480 ps (Fig. 6E). In both cases, the rupture of these interstrand hydrogen bonds gave rise to an increase of interaction energy between the β-strand pairs by 15 kcal/mol (Fig. 7A, B, plots).

Compared to the changes in interaction energy between force bearing β-strands in the case of stretching the T_2T complex, the values recorded during stretching of apo-Z1Z2 are approximately 40% lower. Thus, the results suggest that the intermolecular β-strand interactions between telethonin and Z1Z2 are mechanically stronger than those of the force-bearing intramolecular β-strand interactions of individual Z1 or Z2.

Binding to titin Z1Z2 domains stabilizes telethonin. Previous gene expression studies have shown that telethonin transcripts are not strongly expressed in the absence of titin Z1 and Z2 transcripts (Faulkner et al., 2001). Also, purified telethonin tends to aggregate in solution (Zou et al., 2005), suggesting that telethonin may exist in an altered conformational state when it is unbound to other proteins. It is believed, therefore, that titin Z1 and Z2 play a role in stabilizing the fold of telethonin. In order to examine telethonin's stability, we isolated the telethonin segment (residues 1 to 89) from the structure of the T_2T complex. Equilibration of the telethonin segment alone (simD) over 19.3 ns revealed a large conformational change whereby β-hairpins AB and CD (see Fig. 8A), which bind to titin Z1 and Z2 in the complex, folded

in upon the core of telethonin in the absence of the titin modules. The root mean squared deviation (RMSD) for backbone telethonin atoms jumped immediately to 6 Å within 2.5 ns of equilibration. Over the course of the 19 ns equilibration the RMSD increased to over 8 Å, contributed mainly by the spontaneous unraveling of the AB and CD β-hairpins (Fig. 8B and C). The conformational change to the state observed for free N-terminal telethonin suggests that the upon binding titin in the T_2T complex, telethonin becomes stabilized and constrained.

Discussion

Shifting of the force-bearing component upon telethonin binding. As far as we know from a wide group of examples, the mechanical stability of proteins with mechanical functions is primarily determined by their force-bearing structural element; once this element is ruptured a protein will unravel with little resistance. There exist only few cases where proteins exhibit mechanically stable intermediates that require a second peak force to complete unraveling (Oberhauser et al., 2002; Gao et al., 2002a, 2003). Similar to titin I-band Ig domains I1 and I27 extensively studied previously (Lu et al., 1998; Marszalek et al., 1999; Lu and Schulten, 2000; Gao et al., 2002b,c), the key force-bearing elements of individual Z1 or Z2 are two pairs of β-strands near the protein termini, namely the A and B strands and the A' and G strands. The rupture of interstrand hydrogen bonds between these β-strands induce the transition event to the unfolded state (see Fig. 7). The joining of two Z1Z2 dimers by telethonin creates a configuration where the two Z2 domains transmit force developed in the distal region of the stretched titin molecules. Stretching the C-termini of the Z2 domains in complex with telethonin reveals a shift of the force-bearing element. Compared with the apo-structure, the major force-bearing element of the T_2T complex is the β-strand binding interface between Z2 and telethonin instead of between β-strands within a Z1 or Z2 domain. Specifically, hydrogen bonds between the two G-strands of Z2 (G_{Z2_A} and G_{Z2_B}) and D-and B-strands of telethonin (D_{TLT} and B_{TLT}), respectively, glue the complex together (c.f. Figs. 1, 3, and 4). The key unbinding event corresponds to concurrent breakage of seven backbone hydrogen bonds between G_{Z2_A} and D_{TLT} at the titin-telethonin binding interface. The interaction between these two β-strands is stronger than that between the force-bearing β-strand pairs of individual Z1 or Z2 domains.

Figure 1B demonstrates that the G_{Z2_A} and D_{TLT} interactions are well positioned in the T_2T complex, namely directly adjacent to the $Z2_A$ C-terminus that bears the stretching forces of titin in muscle. Likewise, the C-terminus of $Z2_B$ bears titin stretching forces and, as Fig 1B reveals, a nearby set of interstrand hydrogen bonds linking G_{Z2_B} and B_{TLT} protects T_2T from unravelling. Obviously, this set of hydrogen bonds is even stronger than that linking G_{Z2_A} and D_{TLT}; however once the latter bonds are broken, the T_2T complex rotates such that the stretching forces do not act

anymore in a shearing fashion and bonds are mainly unzipped, one hydrogen bond at a time.

Our simulations also reveal a strengthening of titin Z1Z2 domains against mechanical stretching when complexed with, or molecularly glued together through β-strand cross-linking to telethonin. This finding, that intermolecular hydrogen bonds form the main stabilizing interactions between separate proteins in a complex, reveals a key architectural feature of biological cells performing a mechanical function.

Telethonin as a candidate for the Z-disc titin anchor. Biochemical protein interaction studies have shown that titin Z1 and Z2 domains interact with telethonin in the sarcomeric Z-disc, a structure responsible for anchoring titin to the ends of the sarcomere (Gregorio et al., 1998; Miller et al., 2004). The crystal structure of telethonin in complex with titin Z1Z2 domains reveals a remarkable β-strand cross-linking binding interface that essentially glues together β-strands of Z1 and Z2 domains with those of telethonin (Zou et al., 2005). Since the β-sheets of titin Ig domains have been shown to provide strong mechanical resistance against shearing force developed during stretching of titin (Lu et al., 1998; Lu and Schulten, 2000; Gao et al., 2002a,b), it is tempting to speculate that the intermolecular β-strand cross-linking of the T_2T complex represents likewise a binding interface designed to sustain mechanical stress.

Using molecular dynamics simulations we have examined the stability of titin Z1Z2 and telethonin both individually and in complex. Our results reveal that the T_2T complex is indeed capable of resisting strong stretching forces. Moreover, both constant velocity and constant force SMD simulations suggest that the complex is mechanically more stable than apo-Z1Z2 or the individual Z1 and Z2 domains by themselves. The peak force required to dissociate the complex is twice that required for unfolding the apo-Z1Z2 dimer (see Fig. 2). Similarly, under a constant force of 750 pN, the Z1 domain of the apo-structure became unfolded within 0.5 ns simulation time (Fig. 6), whereas the same magnitude of force does not disrupt the T_2T complex in 2 ns (Fig. 3). This finding suggests that telethonin significantly enhances the mechanical stability of the titin N-terminal Z1Z2 domain.

Self assembly of the titin Z1Z2-telethonin (T_2T) complex. Recent studies on the dynamics of Z-disc proteins such as actin, cypher, FATZ, myotilin and telethonin during muscle growth reveal that only telethonin remains diffusely distributed until the final stages of myofibril maturation (Wang et al., 2005b). These findings are in accordance with prior studies which have found that telethonin transcripts are strongly downregulated in response to denervation (Mason et al., 1999; Schroder et al., 2001; Bonnemann and Laing, 2004), a situation that a developing myofibril may encounter before it is fully innervated during muscle maturation. The appearance of telethonin late in the sequence of muscle growth provides evidence that it likely plays a significant role in the positioning and anchoring of fully assembled titin to the Z-disc during the latter stages of muscle development.

The N-terminal fragment (residue 1 to 89) of telethonin exhibits a structure not unlike that of a bird in flight. Its two wings, β-strands pairs A-B and C-D, extend to form β-sheets with the joining pairs of Z1 and Z2 dimers. Our simulation of isolated telethonin suggests that this particular conformation of the ligand is not stable in the absence of the receptor (see Fig. 8). This result implies that telethonin assumes another unknown conformational state before the binding to titin N-termini, and also, that the binding triggers conformational changes that lead to the functional state of telethonin. Since this binding requires two Z1Z2 segments to be properly positioned at the Z-disc, this may explain why telethonin remains diffusively distributed until titin is assembled in the late stages of myofibril maturation. Our simulation revealing an unstable state for free telethonin is also consistent with existing biochemical evidence that pure telethonin in solution tends to self-aggregate (Zou et al., 2005).

In addition to titin Z1 and Z2, several other proteins have been found to interact with telethonin, and are believed to be involved in maintaining the integrity of the sarcomere by organizing the protein complexes within the Z-disc or regulating muscle growth. These proteins include LIM protein (Knöll et al., 2002; Miller et al., 2004), muscle ankyrin repeat proteins (Kojic et al., 2004; Kontrogianni-Konstantopoulos and Bloch, 2003), FATZ (Faulkner et al., 2001), and myostatin (Nicholas et al., 2002). Muscle-specific LIM protein colocalizes with telethonin residues 53 to 81, and a human MLP mutation (W4R) has been correlated with dilated cardiomyopathy, a pathlology associated with heart failure, a major cause of human morbidity (Knöll et al., 2002; Kojic et al., 2004; Miller et al., 2004). While a structure for MLP is not yet available, the crystal structure for the titin Z1Z2-telethonin complex reveals that residues 53 to 81 of telethonin are not involved in binding titin Z1Z2, but rather, project out slightly from between both sets of titin Z1 and Z2 modules. Thus, it is entirely possible that MLP binds to this projection in a jigsaw puzzle like manner, stabilizing the entire T_2T complex even further. Naturally, it also follows that other Z-disc proteins that have been shown to interact with telethonin may also bind to other regions not involved in the T_2T complex, mainly the C-terminal domain of telethonin which is yet unresolved.

Conclusion

In this work, we have utilized molecular dynamics simulations to study the mechanical basis for titin anchoring at the Z-disc. Telethonin "glues" two titin molecules in antiparallel arrangement around itself by forming a heterotrimeric complex. The simulations revealed that the complex is mechanically very strong, even more resistant to stretching forces than the Z1 and Z2 domains by themselves. This result provides strong evidence that telethonin plays an important role as a titin anchor.

Beyond this finding specific for muscle, our simulations reveal also a fundamental architectural element of living cells, namely, how cells glue their components together yielding strong mechanical connections. The structural motifs employed by telethonin in this respect, namely, cross-linking β-strands, has also been implicated in

fibril formation (Louis et al., 2005) and it is important to take note of such potential pathological side effects of telethonin's motif. Clearly, the deployment of telethonin needs to be carefully controlled in the cell and future work will likely focus on the control mechanisms used in focusing telethonin and similar other, yet unknown, mechanical proteins on gluing the right protein components, and not the wrong ones, in particular, to avoid self-aggregation.

Experimental Procedures

Simulated Systems. Atomic coordinates of the titin Z1Z2-telethonin (T_2T) complex were taken from the crystal structure (Protein Data Bank entry code 1YA5 (Zou et al., 2005)). The structure consists of three individual protein segments - two separate titin N-terminal Z1Z2 segments named ZA (residues 1 to 197) and ZB (residues 1 to 198), which are joined together by one N-terminal telethonin (TLT) fragment (residues 1 to 89). The topology of the complex and missing hydrogen atoms were generated using psfgen (Phillips et al., 2005) with the topology file for CHARMM27 (MacKerell Jr. et al., 1998). For the present MD study, four simulation systems were derived from this model.

In the first system, for simulating the T_2T complex, a water box with dimension $96 \times 86 \times 213$ Å^3 was used to solvate the system. The system size totaled 107,946 atoms, consisting of 484 protein residues (7,374 atoms) and 33,524 water molecules (100,572 atoms). The second and third systems contain only a single titin Z1Z2 peptide derived from the ZA segment ($Z1Z2_A$), and solvated in two water boxes with two different sizes, a smaller one of size $41 \times 59 \times 129$ Å^3 for an equilibrium study and a larger one of size $281 \times 73 \times 68$ Å^3 in order to accommodate the extension of the protein during stretching in SMD simulations. These systems contain 35,762 atoms and 131,189 atoms, respectively. In the fourth system, the telethonin fragment was isolated from the complex and solvated in a water box with dimensions $74 \times 72 \times 126$ Å^3, resulting in a system size of 64,356 atoms.

Molecular Dynamics. Simulations were performed using NAMD 2.5 (Phillips et al., 2005) with the CHARMM27 force field for proteins (MacKerell Jr. et al., 1998) and the TIP3P model (Jorgensen et al., 1983) for explicit water molecules. Particle Mesh Ewald (PME) summation was employed to calculate long-range electrostatic forces with a grid size of less than 1 Å. Van der Waals interactions employed a switching function starting at 10 Å and a cutoff of 12 Å. An integration time step of 1 fs was adopted, with a multiple time-stepping algorithm (Grubmüller et al., 1991; Schlick et al., 1999) employed to compute covalent bonds every time step, short-range nonbonded interactions every two time steps, and long range electrostatic forces every four time steps. Multiple time-stepping increases the efficiency of simulation by a factor of two, making the nanosecond time scale accessible for our simulations. Constant temperature control (T=300 K) was employed using Langevin dynamics for NVT and NPT ensemble simulations to control the kinetic energy of the system. A Langevin coupling coefficient of 5 ps^{-1} was used for the temperature control. Constant pressure simulations (NPT) at P = 1 atm (101.3kPa) utilized the Nosé-Hoover Langevin piston method with a decay period of 100 fs and a damping time constant of 50 fs. During NPT simulations, the size of the simulated periodic box was allowed to freely change.

Steered molecular dynamics (SMD) simulations (Izrailev et al., 1998; Isralewitz et al., 2001) were carried out by either fixing the C_α atom of the C-terminus of one titin segment (ZA) and applying an external force to the C-terminal C_α atom of another

titin segment (ZB), or applying an external force simultaneously to the terminal C_α of two termini along opposite directions (see figures in the Results section for stretching configurations). The directions were in parallel to the vector connecting two stretched termini. Both constant velocity and constant force protocols were employed. For constant velocity SMD, the pulled atom is harmonically constrained with a force $F = -k(x - vt)$ where k represents the spring constant, and x, v, and t the coordinate, velocity, and the time, respectively. Whereas constant velocity SMD features an increasing force along time, constant force applies a time-independent potential of $F = kx$ to the specified atom(s), where x is the atom-atom distance. For the spring constant, we chose a value of $3k_B\mathrm{T}/\mathrm{\AA}^2$ which corresponds to an rmsd value of $\sqrt{k_BT/k} \approx 0.5\mathrm{\AA}$.

Analysis. System coordinates were saved every picosecond, and analysis was performed using the program VMD (Humphrey et al., 1996). The structural changes to proteins were monitored by calculating the root mean squared deviation (RMSD) of their backbone atoms. The end-to-end distance profile of a stretched system is based on the distance between the two stretched or between the stretched and fixed terminal C_α atoms. The change of the end-to-end distance is defined as the extension of the system. Hydrogen bonds were calculated in VMD with a distance cutoff of 3.0 Å for bonding pairs. The interaction energy between β-strands was calculated using the NAMD pairwise interaction energy analysis module.

Summary of Simulations. A detailed summary of simulations carried out is provided in Table 1. The equilibration of the four systems (simA1, simC1, simC2, and simE) followed an identical procedure. A system is first minimized for 2000 conjugate gradient steps, then equilibrated in a 300 K heat bath with constant volume for 15 ps. Following this, the temperature control was released and the entire system equilibrated under NPT conditions. The equilibration time varies from 1 ns to 28 ns (see Table 1). All steered molecular dynamics (SMD) simulations utilized the equilibrated apo-Z1Z2 structure from simC2 or the equilibrated T_2T complex structure from simA1. For constant velocity simulations, a velocity of 0.05 Å/ps was employed. In constant force simulations, forces of 750, 1000, 1200, and 1500 pN were used. The SMD parameters are listed in Table 1.

Simulations were conducted on the Teragrid and SGI Altix supercomputing clusters at the National Center for Supercomputing Applications (NCSA) at the University of Illinois at Urbana-Champaign. A system of 100,000 atoms requires one day of computing for 3 ns on 64 1.6Ghz Itanium 2 processors. The total simulation times reported in this study included 17 ns for the T_2T complex (108,000 atoms), 42 ns for apo titin Z1Z2 alone (36,000 and 131,000 atoms), and 19 ns for telethonin alone (64,000 atoms).

Acknowledgements

We wish to thank Olga Mayans for helpful discussions. This work was supported by the National Institutes of Health (NIH P41-RR05969). Computer time was provided through support from the National Resource Allocation Committee grant (NRAC MCA93S028) from the National Science Foundation.

References

Bonnemann, C., and Laing, N. (2004). The novel sarcomeric protein telethonin exhibits developmental and functional regulation. Curr. Op. Neur. *17*, 529–537.

Craig, D., Gao, M., Schulten, K., and Vogel, V. (2004). Tuning the mechanical stability of fibronectin type III modules through sequence variation. Structure *12*, 21–30.

Erickson, H. (1997). Stretching single protein modules: Titin is a weird spring. Science *276*, 1090–1093.

Faulkner, G., Lanfranchi, G., and Valle, G. (2001). Telethonin and other new proteins of the Z-disc of skeletal muscle. Life *51*, 275–282.

Furst, D., Osborn, M., Nave, R., and Weber, K. (1988). The organization of titin filaments in the half-sarcomere revealed by monoclonal antibodies in immuno-electron microscopy - a map of 10 non-repetitive epitopes starting at the z-line extends to the m-line. J. Cell Biol. *106*, 1563–1572.

Furukawa, T., Ono, Y., Tsuchiya, H., Katayama, Y., Bang, M., Labeit, D., Labeit, S., Inagaki, N., and Gregorio, C. (2001). Specific interaction of potassium channel β-subunit mink with the sarcomeric protein T-cap suggests a T-tubule-myofibril linking system. J. Mol. Biol. *313*, 775–784.

Gao, M., Craig, D., Lequin, O., Campbell, I.D., Vogel, V., and Schulten, K. (2003). Structure and functional significance of mechanically unfolded fibronectin type III1 intermediates. Proc. Natl. Acad. Sci. USA *100*, 14784–14789.

Gao, M., Craig, D., Vogel, V., and Schulten, K. (2002a). Identifying unfolding intermediates of FN-III_{10} by steered molecular dynamics. J. Mol. Biol. *323*, 939–950.

Gao, M., Lu, H., and Schulten, K. (2002b). Unfolding of titin domains studied by molecular dynamics simulations. J. Muscle Res. Cell Mot. *23*, 513–521.

Gao, M., Wilmanns, M., and Schulten, K. (2002c). Steered molecular dynamics studies of titin I1 domain unfolding. Biophys. J. *83*, 3435–3445.

Gautel, M., Goulding, D., Bullard, B., Weber, K., and Furst, D.O. (1996). The central Z-disk region of titin is assembled from a novel repeat in variable copy numbers. J. Cell. Sci. *109*, 2747–2754.

Granzier, H.L., and Labeit, S. (2004). The giant protein titin a major player in myocardial mechanics, signaling and disease. Circulation Res. *94*, 284–295.

Gräter, F., Shen, J., Jiang, H., Gautel, M., and Grubmüller, H. (2005). Mechanically induced titin kinase activation studied by force-probe molecular dynamics simulations. Biophys. J. *88*, 790–804.

Gregorio, C.C., Trombitas, K., Centner, T., Kolmerer, B., Stier, G., Kunke, K., Suzuki, K., Obermayr, F., Herrmann, B., Granzier, H., et al. (1998). The NH2 terminus of titin spans the Z-disc: Its interaction with a novel 19-kD ligand (T-cap) is required for sarcomeric integrity. J. Cell Biol. *143*, 1013–1027.

Grubmüller, H., Heller, H., Windemuth, A., and Schulten, K. (1991). Generalized Verlet algorithm for efficient molecular dynamics simulations with long-range interactions. Mol. Sim. *6*, 121–142.

Humphrey, W., Dalke, A., and Schulten, K. (1996). VMD – Visual Molecular Dynamics. J. Mol. Graphics *14*, 33–38.

Isralewitz, B., Gao, M., and Schulten, K. (2001). Steered molecular dynamics and mechanical functions of proteins. Curr. Op. Struct. Biol. *11*, 224–230.

Itoh-Satoh, M., Hayashi, T., Nishi, H., Koga, Y., Arimura, T., Koyanagi, T., Takahashi, M., Hohda, S., Ueda, K., Nouchi, T., et al. (2002). Titin mutations as the molecular basis for dilated cardiomyopathy. Biochem. Biophys. Res. Commun. *291*, 385–393.

Izrailev, S., Stepaniants, S., Isralewitz, B., Kosztin, D., Lu, H., Molnar, F., Wriggers, W., and Schulten, K. (1998). Steered molecular dynamics. In P. Deuflhard, J. Hermans, B. Leimkuhler, A. E. Mark, S. Reich, and R. D. Skeel, editors, *Computational Molecular Dynamics: Challenges, Methods, Ideas*, volume 4 of *Lecture Notes in Computational Science and Engineering*. Springer-Verlag, Berlin, 39–65.

Jorgensen, W.L., Chandrasekhar, J., Madura, J.D., Impey, R.W., and Klein, M.L. (1983). Comparison of simple potential functions for simulating liquid water. J. Chem. Phys. *79*, 926–935.

Karanicolas, J., and Brooks, C. (2003). The structural basis for biphasic kinetics in the folding of the ww domain from a formin-binding protein: lessons for protein design. Proc. Natl. Acad. Sci. USA *100*, 3555–3556.

Knöll, R., Hoshijima, M., Hoffman, H., Person, V., Lorenzen-Schmidt, I., Bang, M., Hayashi, T., Shiga, N., Yasukawa, H., Schaper, W., et al. (2002). The cardiac mechanical stretch sensor machinery involves a Z disc complex that is defective in a subset of human dilated cardiomyopathy. Cell *111*, 943–955.

Kojic, S., Medeot, E., Guccione, E., Krmac, H., Zara, I., Martinelli, V., Valle, G., and Faulkner, G. (2004). The Ankrd2 protein, a link between the sarcomere and the nuclear in skeletal muscle. J. Mol. Biol. *339*, 313–325.

Kontrogianni-Konstantopoulos, A., and Bloch, R.J. (2003). The hydrophilic domain of small ankyrin-1 interacts with the two n-terminal immunoglobulin domains of titin. J. Biol. Chem. *278*, 3985–3991.

Lange, S., Xiang, F., Yakovenko, A., Vihola, A., Hackman, P., Rostkova, E., Kristensen, J., Brandmeier, B., Franzen, G., Hedberg, B., et al. (2005). The kinase domain of titin controls muscle gene expression and protein turnover. Science *308*, 1599–1603.

Laval, S., and Bushby, K. (2004). Limb-girdle muscular dystrophies - from genetics to molecular pathology. Neurpath. & Appl. Neurobiol. *30*, 91–105.

Linke, W. (2000). Stretching molecular springs: elasticity of titin filaments in vertebrate striated muscle. Histol Histolpath. *15*, 799–811.

Louis, J., Byeon, I., Baxa, U., and Gronenborn, A. (2005). The gb1 amyloid fibril: recruitment of the peripheral β-strands of the domain swapped dimer into the polymeric interface. J. Mol. Biol. *348*, 687–698.

Lu, H., Isralewitz, B., Krammer, A., Vogel, V., and Schulten, K. (1998). Unfolding of titin immunoglobulin domains by steered molecular dynamics simulation. Biophys. J. *75*, 662–671.

Lu, H., and Schulten, K. (1999). Steered molecular dynamics simulations of force-induced protein domain unfolding. Proteins: Struct., Func., Gen. *35*, 453–463.

Lu, H., and Schulten, K. (2000). The key event in force-induced unfolding of titin's immunoglobulin domains. Biophys. J. *79*, 51–65.

MacKerell Jr., A.D., Bashford, D., Bellott, M., Dunbrack Jr., R.L., Evanseck, J., Field, M.J., Fischer, S., Gao, J., Guo, H., Ha, S., et al. (1998). All-atom empirical potential for molecular modeling and dynamics studies of proteins. J. Phys. Chem. B *102*, 3586–3616.

Marszalek, P.E., Lu, H., Li, H., Carrion-Vazquez, M., Oberhauser, A.F., Schulten, K., and Fernandez, J.M. (1999). Mechanical unfolding intermediates in titin modules. Nature *402*, 100–103.

Maruyama, K. (1997). Connectin/titin, a giant elastic protein of muscle. FASEB J. *11*, 341–345.

Mason, P., Bayol, S., and Loughna, P. (1999). The novel sarcomeric protein telethonin exhibits developmental and functional regulation. Biochem. Biophys. Res. Commun. *257*, 699–703.

Miller, M., Granzier, H., Ehler, E., and Gregorio, C. (2004). The sensitive giant: the role of titin-based stretch sensing complexes. Trends Cell. Biol. *14*, 119–126.

Mues, A., van der Ven, P.F.M., Young, P., Furst, D.O., and Gautel, M. (1998). Two immunoglobulin-like domains of the z-disc portion of titin interact in a conformation-dependent way with telethonin. FEBS Lett. *428*, 111–114.

Nicholas, G., Thomas, M., Langley, B., Somers, W., Patel, K., Kemp, C., Sharma, M., and Kambadur, R. (2002). Titin-cap associates with, and regulates secretion of, myostatin. J. Cell. Phys. *193*, 120–131.

Oberhauser, A., Badilla-Fernandez, C., Carrion-Vazquez, M., and Fernandez, J. (2002). The mechanical hierarchies of fibronectin observed with single molecule AFM. J. Mol. Biol. *319*, 433–447.

Obermann, W., Gautel, M., Weber, K., and Furst, D. (1997). Molecular structure of the sarcomeric m band: mapping of titin and myosin binding domains in myomesin and the identification of potential regulatory phosphorylation site in myomesin. EMBO J. *16*, 211–220.

Phillips, J.C., Braun, R., Wang, W., Gumbart, J., Tajkhorshid, E., Villa, E., Chipote, C., Skeel, R.D., Kale, L., and Schulten, K. (2005). Scalable molecular dynamics with NAMD. J. Comp. Chem. *26*, 1781–1802.

Pyle, W.G., and Solaro, R.J. (2004). At the crossroads of myocardial signaling - the role of Z-discs in intracellular signaling and cardiac function. Circulation Res. *94*, 296–305.

Rief, M., Gautel, M., Oesterhelt, F., Fernandez, J.M., and Gaub, H.E. (1997). Reversible unfolding of individual titin immunoglobulin domains by AFM. Science *276*, 1109–1112.

Schlick, T., Skeel, R., Brünger, A., Kalé, L., Board Jr., J.A., Hermans, J., and Schulten, K. (1999). Algorithmic challenges in computational molecular biophysics. J. Comp. Phys. *151*, 9–48.

Schroder, R., Reimann, J., Iakovenko, A., Mues, A., Bonnemann, C., Matten, J., and Gautel, M. (2001). Early and selective disappearance of telethonin protein from the sarcomere in neurogenic atrophy. J. Muscle Res. Cell Mot. *22*, 259–264.

Tjernberg, L., Callaway, D., Tjernberg, A., Hahne, S., Lilliehook, C., Terenius, L., Thyberg, J., and Nordstedt, C. (1999). A molecular model of alzheimer amyloid beta-peptide fibril formation. J. Biol. Chem. *274*, 12619–12625.

Tskhovrebova, L., and Trinick, J. (2003). Titin: Properties and family relationships. Nat. Rev. Mol. Cell. Biol. *4*, 679–689.

Vainzof, M., Moreira, E., Suzuki, O., Faulkner, G., Valle, G., Beggs, A., Carpen, O., Ribeiro, A., Zanoteli, E., Gurgel-Gianneti, J., et al. (2002). Telethonin protein expression in neuromuscular disorders. Biochim. Biophys. Acta *1588*, 33–40.

Valle, G., Faulkner, G., DeAntoni, A., Pacchioni, P., Pallavicini, A., Pandolfo, D., Tiso, N., Toppo, S., Trevisan, S., and Lanfranchi, G. (1997). Telethonin, a novel sarcomeric protein of heart and skeletal muscle. FEBS Lett. *415*, 163–168.

Walsh, D., Hartley, D., Condron, M., Selkoe, M., and Teplow, D. (2001). In vitro studies of amyloid beta-protein fibril assembly and toxicity provide clues to the aetiology of flemish variant (ala692–¿gly) alzheimer's disease. Biochem. J. *355*, 869–877.

Wang, J., G"ulich, S., Bradford, C., Ramirez-Avarado, M., and Regan, L. (2005a). A twisted four-sheeted model for an amyloid fibril. Structure *13*, 1279–1288.

Wang, J., Shaner, N., Mittah, B., Zhou, Q., Chen, J., Sanger, J., and Sanger, J. (2005b). Dynamics of Z-band based proteins in developing skeletal muscle cells. Cell Mot. & Cytoskel. *61*, 34–48.

Wang, K. (1996). Titin/connectin and nebulin: Giant protein ruler of muscle structure and function. Adv. Biophys. *33*, 123–134.

Zou, P.J., Pinotsis, N., Marino, M., Lange, S., Popov, A., Mavridis, I., Gautel, M., Mayans, O.M., and Wilmanns, M. (2005). Molecular basis of telethonin-mediated linkage of the N-terminus of titin within the sarcomeric Z-disc. Nature , in press.

Legends to figures

Figure 1. Structure of titin Z1Z2-telethonin (T_2T) complex and setup for MD simulations. (A) Cartoon representation of two separate N-terminal titin Z1Z2 Ig-domains joined by one N-terminal telethonin (TLT) molecule fragment (residues 1 to 89). Two titin molecules are individually colored blue and red (Z_A and Z_B, respectively). TLT is colored in yellow. The β-strands involved in critical force bearing contacts for each titin Ig-domain (AB and A'G) and between each titin Z2 module and telethonin are labeled (GB and GD). Unless otherwise noted, the same color scheme was adopted in all figures of this manuscript. (B) Detailed schematic of β-strand alignment for the T_2T complex, with force bearing hydrogen bonds shown for β-strand pairs AB and A'G for titin domains, and hydrogen bonds linking G_{Z1_A}, G_{Z2_B}, G_{Z1_B}, G_{Z2_A} on the Ig domains to A_{TLT}, B_{TLT}, C_{TLT}, D_{TLT}, on telethonin, respectively. The naming scheme shown for β-strands of apo-Z1Z2 and the T_2T complex corresponds to that adopted in the text. (C) Surface view of the solvated T_2T ensemble, illustrating the extensive contact and interdigitation of TLT β-sheet domains between opposing titin molecules. In all simulations described below, a simulated protein or complex was solvated in an explicit water cell with appropriate size (see Methods).

Figure 2. Mechanical stability comparison between a non-ligand-bound Z1Z2 dimer (apo-Z1Z2) and telethonin-liganded titin Z1Z2 complex. In both cases, the equilibrated structures were stretched with a harmonic spring moving at a constant velocity of 0.05Å/ps. Unbinding the complex requires significantly higher force than unfolding the apo-Z1Z2 peptide, as shown in the force *vs.* extension profiles obtained from the simulations. The extension is defined as the change of the end-to-end distance between the two termini which were either fixed in space or pulled with the harmonic force. The complex shown in (A) defines the equilibrated T_2T complex structure and the pulling configuration for simA2. (B) At extension of 15Å, a peak force of nearly 2000 pN is necessary for detaching the β-strand G_{Z2_A} from its cross-linkcross-linking partner, β-strand D_{TLT}. (C) The $Z2_A$ domain becomes separated from the ligand at extension 25 Å. (D) Unraveling the A_{Z2_A} of the Ig domain leads to further separation. In snapshots A–D, the color code is the same as defined in Fig. 1, except that the four G-strands forming β-strands with telethonin are colored in grey. Snapshots of apo-Z1Z2 (E) at the beginning of stretching (simC3), (F) right after the unfolding peak force at extension of 35 Å, where the β-strands A- and A'- of Z2 begin to separate from the fold, and (G) at extension of 50 Å, where A- and A'-strands of Z2 become detached. The two β-sheets of each titin domain for (E)-(G) are shown in green (A'CC'FG) and blue (ABED), except that β-strands A and A' of Z1 are shown in red and orange, respectively.

Figure 3. Forced unbinding of the titin Z1Z2-telethonin complex. Shown in the plot is the distance between two stretched titin Z2 α-carbon termini during constant

force SMD simulations (simB1-simB4) at forces of 750 pN (blue), 1000 pN (green), 1200 pN (red), and 1500 pN (black), respectively. Forces of 750 pN and 1000 pN could not separate the complex within the simulation time, whereas forces of 1200 pN and 1500 pN were sufficient to detach titin Z2 from telethonin. Snapshots taken from the unbinding trajectory of the 1200 pN simulation represent (A) the initial equilibrated structure, (B) and (C) the transition events where β-strands G_{Z2_A} and G_{Z2_B} (colored in grey) separate from β-strands D_{TLT} and B_{TLT}, respectively, and (D) the detachment and unfolding of the $Z2_A$ domain, causing rapid extension of the complex.

Figure 4. The force-bearing inter-molecule β-strands involved in key hydrogen bond breakage events for β-strands between titin Z2 (G_{Z2_A}) and telethonin (D_{TLT}). A hydrogen bond cutoff distance 3 Å was employed, with stable hydrogen bonds shown as thick dashed lines and broken hydrogen bonds shown as thin dashed lines. Snapshots of the strands are taken from the 1200pN constant force SMD simulation presented in Figure 3. (A) The pair of β-strands with seven stably formed backbone hydrogen bonds at the initial equilibrium state. (B) Rupture of these hydrogen bonds at 438 ps leads to a concomitant increase in β-strand pair interaction energy shown in the plot. (C) Three broken hydrogen bonds reformed at the 470 ps, correlating to a temporary decrease in interaction energy. However, with continued stretching (D) the two β-strand fully separate at the 526 ps. The inset plot presents a running count (blue) of all hydrogen bonds between backbone atoms formed between the two β-strands; the decrease in the number of formed hydrogen bonding pairs is correlated with a decrease in stability when viewed against the interaction energy profile (green).

Figure 5. Equilibration of titin Z1Z2 in the absence of telethonin over 28 ns reveals that individual titin Z1 and Z2 domains are structurally stable. Backbone RMSD of individual Z1 (black) and Z2 (red) domains show little deviation from the bound crystal structure; however, the backbone RMSD of both titin Z1Z2 combined (green) shows a significant deviation associated with the displacement of titin Z1 relative to titin Z2 connected via a flexible linker region. The inset figure shows titin Z1Z2 overlapped with its own image at the beginning (t=0 ns) and end (t=28 ns) of the simulation.

Figure 6. Response of the apo-Z1Z2 dimer to a constant stretching force. (A) A force of 750 pN is applied to the C_α atoms of the N-terminal and the C-terminal residues of the molecule in the opposite directions. (B) The detachment of β-strand A from β-strand B of Z1 is followed by (C) the separation of the same two β-strands (A-B) of Z2. (D) The unraveling of the β-strand A' of Z1 detach leads to (E) a rapid extension of the complex. The inset shows the plot of N to C terminal distance of the dimer *vs.* time. The color scheme used for the β-strands is the same as used in Fig. 2.

Figure 7. Key β-strand interactions contributing to the unfolding barrier for apo-Z1Z2. Shown in (A) and (B) are representative snapshots which reveal the separation of β-strands pairs AB and A'G on both Z1 and Z2 as the dimer is stretched under a 750 pN constant force. The time points represented in this figure correspond to the events shown in Fig 6. For each Ig domain, the equilibrated β-strand pairs are presented with stably formed backbone hydrogen bonds (thick dashed lines). As the protein is stretched, these β-strands separate and broken hydrogen bonds are then shown by thin dashed lines. (A) Interstrand hydrogen bonds between A- and B-strands and between A'- and G-strands of Z1 are broken under tension at 120 ps and 380 ps, respectively. (B) illustrates the rupture of six A-B hydrogen bonds and five A'-G bonds of Z2. The disruption of these critical bonds is responsible for the increase of instability seen on the accompanying plots of β-strand pair interaction energy over the course of the simulations.

Figure 8. Instability of free telethonin. An equilibration simulation of an N-terminal telethonin segment over 19 ns (simD) reveals a large conformational change of the structure. The gradual bending of two β-hairpins of telethonin can be seen in (A) the series of snapshots at (i) 0 ps, (ii) 2.5 ns, (iii) 8 ns, and (iv) 12 ns. (B) The backbone RMSD along the entire 20 ns trajectory shows that the telethonin N-terminal fragment exhibits a large conformational change in the absence of Z1Z2 titin. (C) The average RMSD per residue over the entire trajectory shows two peaks that reveal increased motion of the two β-sheet projections (labeled AB and CD) that are seen to fold upwards in (A). The third peak reflects a slight bending of the β-sheet formed by strands E and F.

name	structure	type	ensemble	atoms $\times 1000$	size Å^3	SMD parameters	time ns
simA1	Z1Z2-TLT	EQ	NpT	108	$96 \times 86 \times 213$	–	1.0
simA2	Z1Z2-TLT	SCV	NV	108	$96 \times 86 \times 213$	0.05 Å/ps[a]	2.0
simB1	Z1Z2-TLT	SCF	NV	108	$96 \times 86 \times 213$	750 pN[b]	2.0
simB2	Z1Z2-TLT	SCF	NV	108	$96 \times 86 \times 213$	1000 pN[b]	2.0
simB3	Z1Z2-TLT	SCF	NV	108	$96 \times 86 \times 213$	1200 pN[b]	1.0
simB4	Z1Z2-TLT	SCF	NV	108	$96 \times 86 \times 213$	1500 pN[b]	1.0
simB5	Z1Z2-TLT	SCF	NV	108	$96 \times 86 \times 213$	750 pN[a]	2.0
simB6	Z1Z2-TLT	SCF	NV	108	$96 \times 86 \times 213$	1200 pN[a]	1.0
simC1	Z1Z2	EQ	NpT	36	$41 \times 59 \times 129$	–	27.8
simC2	Z1Z2	EQ	NpT	131	$281 \times 73 \times 68$	–	10.0
simC3	Z1Z2	SCV	NV	131	$281 \times 73 \times 68$	0.05Å/ps[c]	1.0
simC4	Z1Z2	SCF	NV	131	$281 \times 73 \times 68$	750 pN[d]	3.0
simD	TLT[f]	EQ	NpT	64	$74 \times 72 \times 126$	–	19.3

[a]Fixed C-term. C_α atom of titin $Z2_B$; pull C-term. C_α atom of titin $Z2_A$.
[b]Pull both Z2 termini C_α atoms.
[c]Fixed N-terminal C_α atom on Z1, pull C-terminal C_α atom on Z2.
[d]Pull both C_α atom of N-terminal Z1 and C-terminal Z2.
[f]Residues 1 to 89.

Table 1: Summary of simulations. Under "type", EQ denotes equilibration; S denotes steered molecular dynamics (SMD) simulations, with CV and CF corresponding to constant velocity and constant force conditions, respectively. The "ensemble" column lists the variables held constant during the simulations; N, V, p, and T correspond to number of atoms, volume, pressure, and temperature, respectively. Footnotes under SMD parameters describe which atoms were fixed or had an external force applied to them.

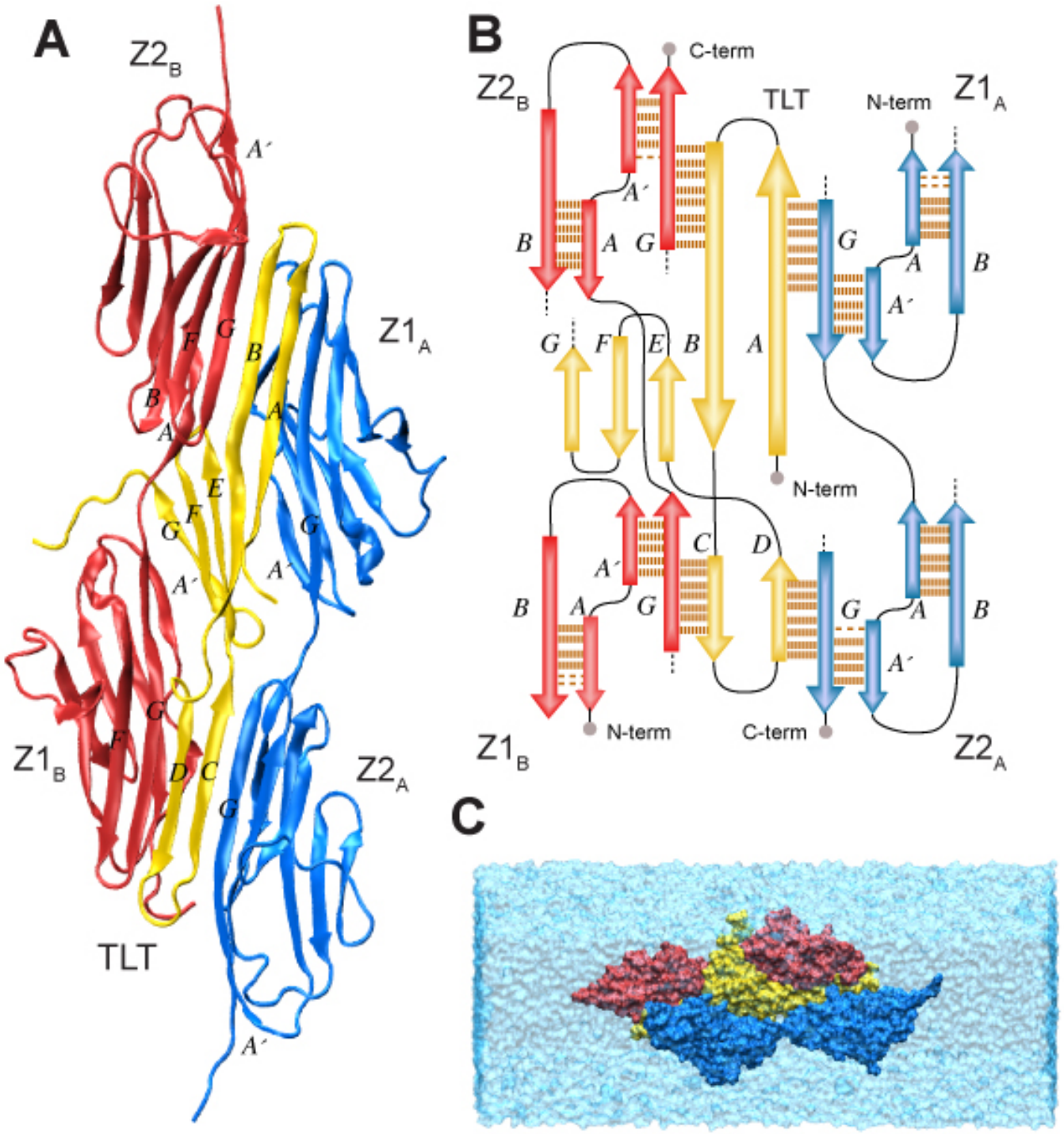
A
Z2B
Z1A
Z1B
Z2A
TLT
B
C-term
N-term
C
Figure 1:

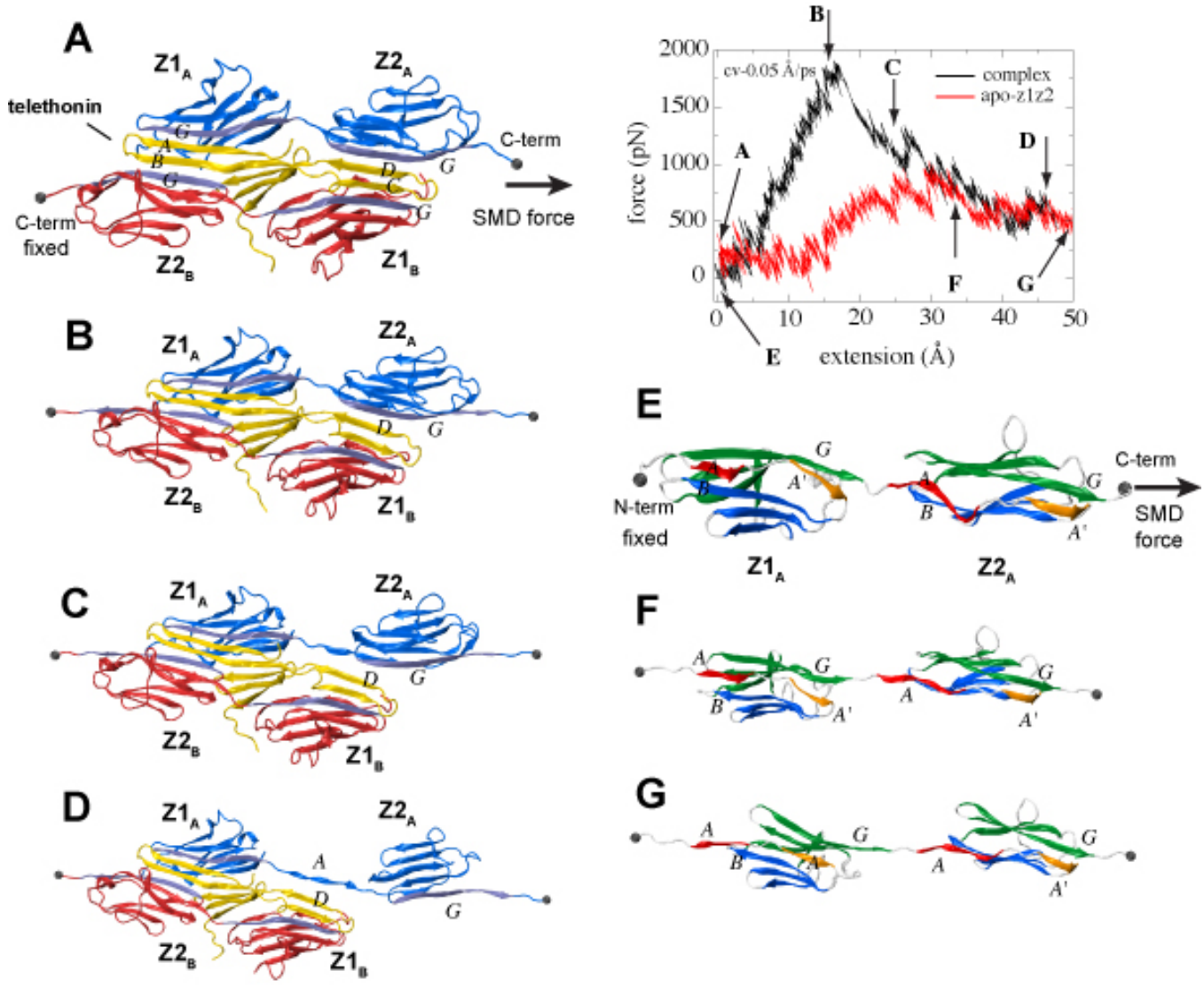
A
telethonin
Z1A
Z2A
C-term
fixed
SMD force
Z2B
Z1B
B
C
D
E
N-term
fixed
C-term
SMD force
F
G
cv-0.05 Å/ps
complex
apo-z1z2
force (pN)
extension (Å)

Figure 2:

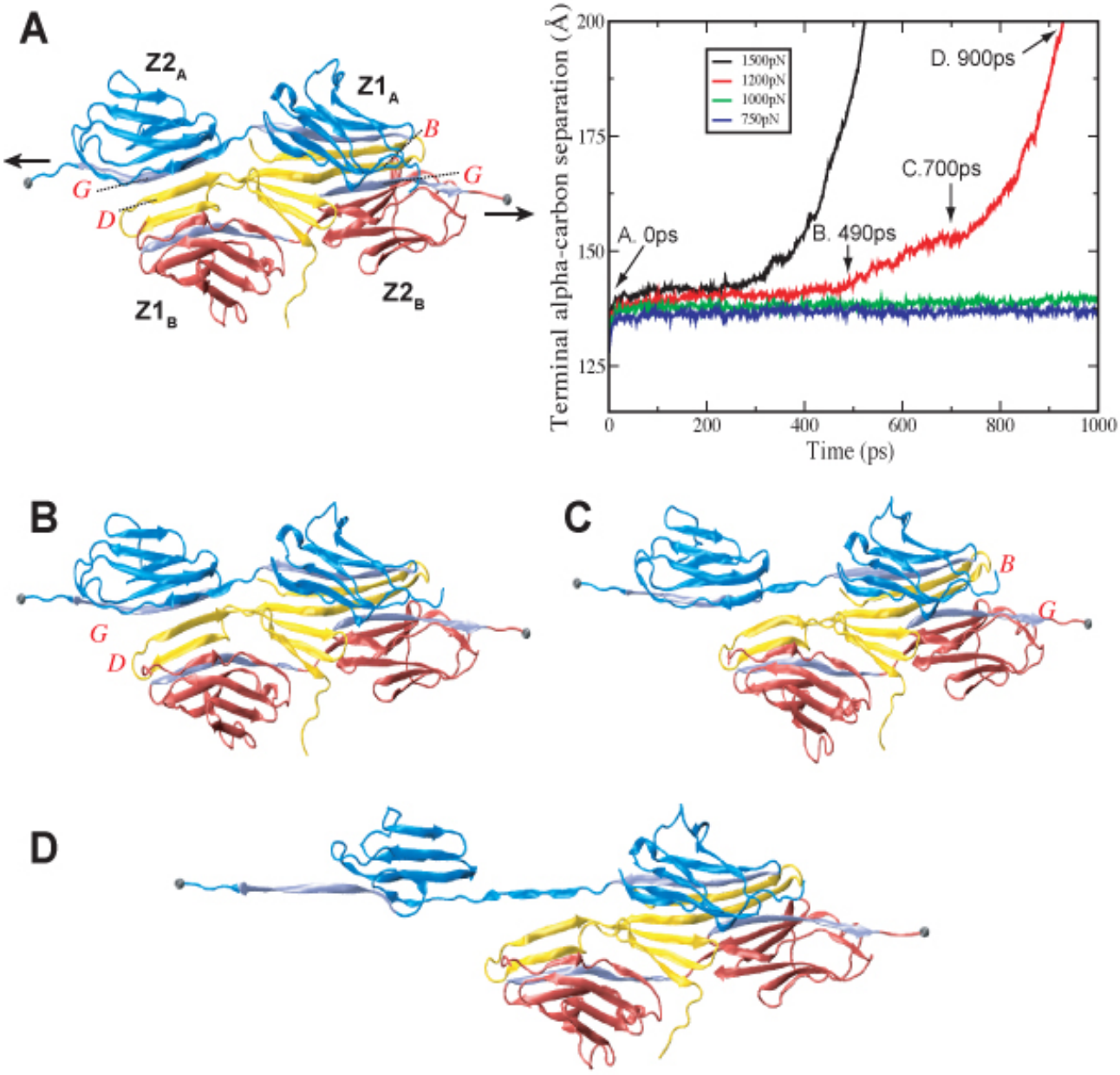
A
Z2A
Z1A
B
G
G
D
Z1B
Z2B
1500pN
1200pN
1000pN
750pN
D. 900ps
C.700ps
A. 0ps
B. 490ps
Terminal alpha-carbon separation (Å)
Time (ps)
200
175
150
125
0
200
400
600
800
1000
B
G
D
C
B
G
D

Figure 3:

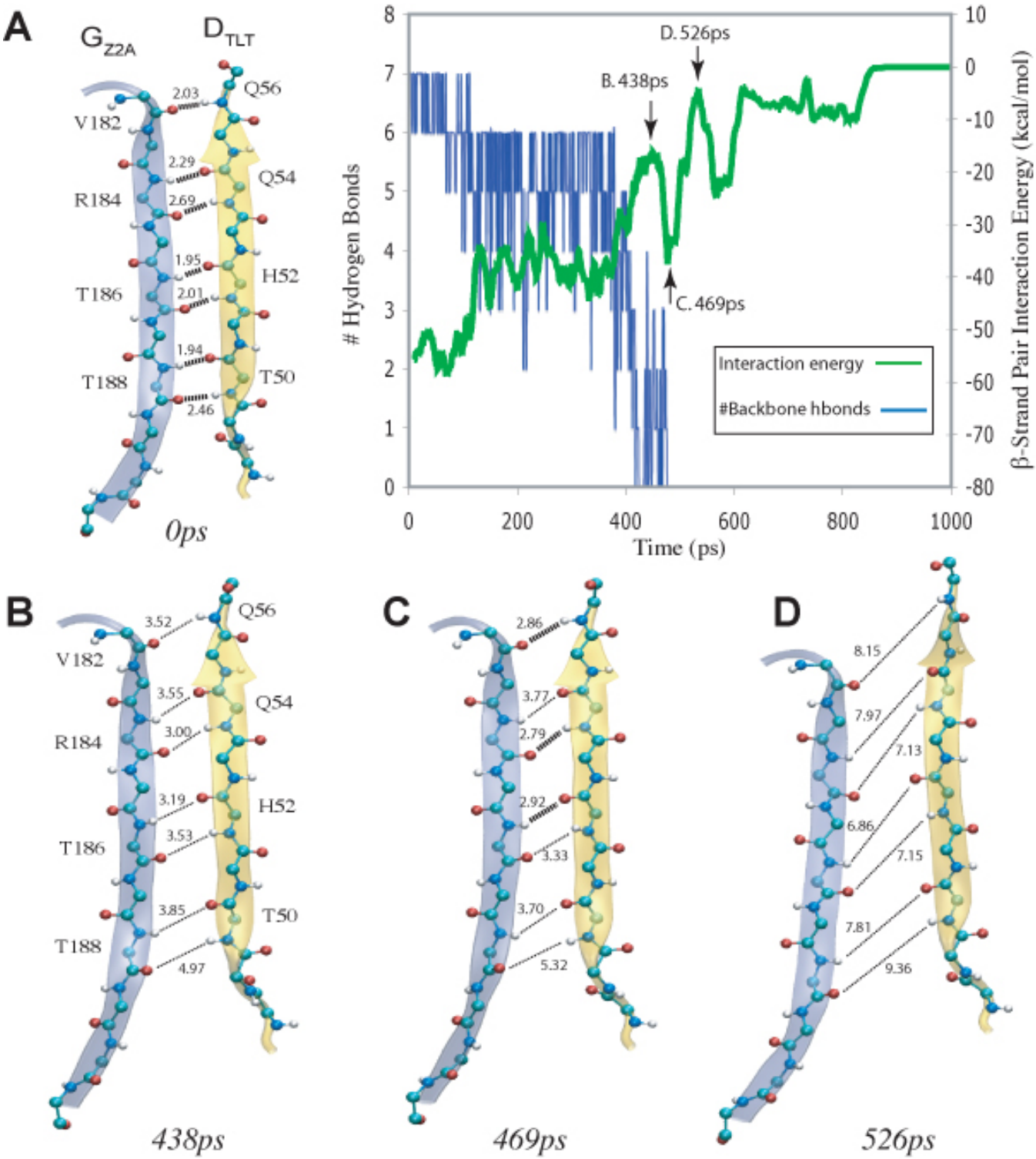
A
G Z2A
D TLT
Q56
V182
Q54
R184
H52
T186
T50
T188
2.03
2.29
2.69
1.95
2.01
1.94
2.46
0ps
D. 526ps
B. 438ps
C. 469ps
Hydrogen Bonds
β-Strand Pair Interaction Energy (kcal/mol)
Time (ps)
Interaction energy
#Backbone hbonds
B
3.52
3.55
3.00
3.19
3.53
3.85
4.97
438ps
C
2.86
3.77
2.79
2.92
3.33
3.70
5.32
469ps
D
8.15
7.97
7.13
6.86
7.15
7.81
9.36
526ps

Figure 4:

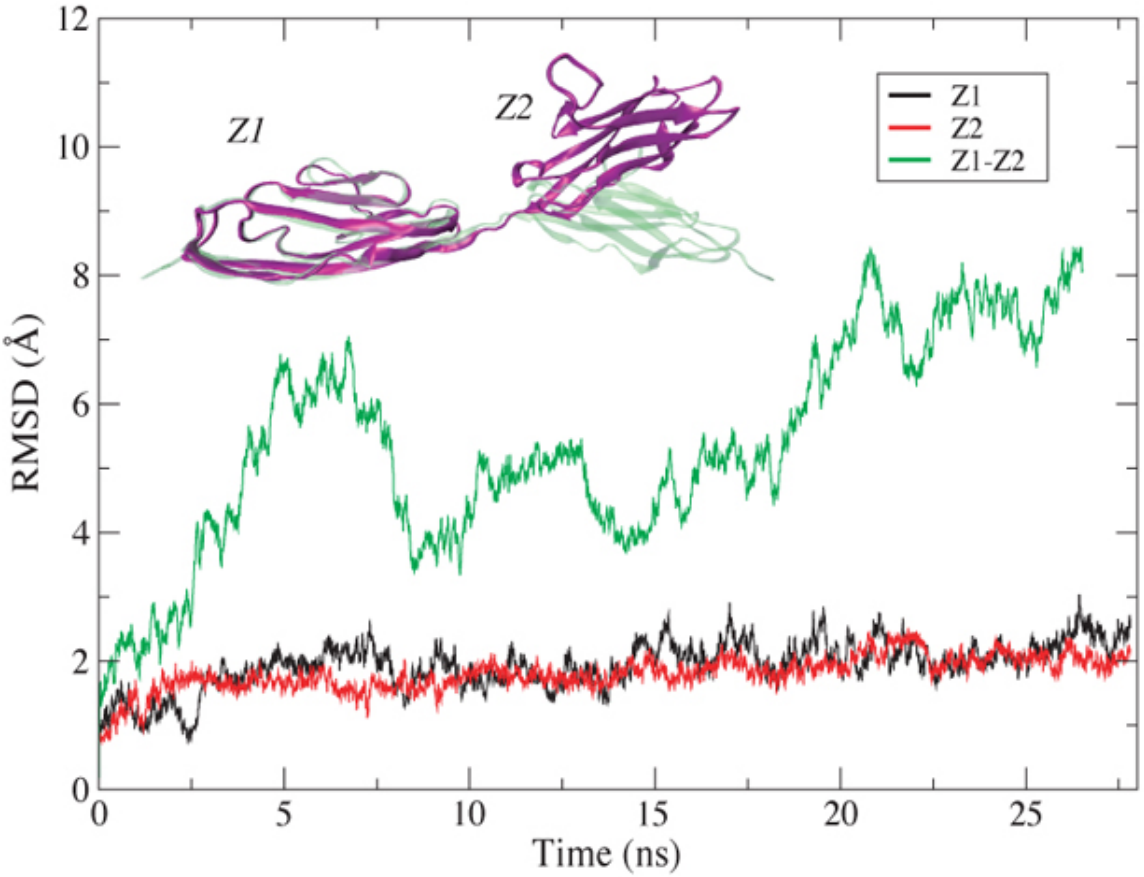

Figure 5:

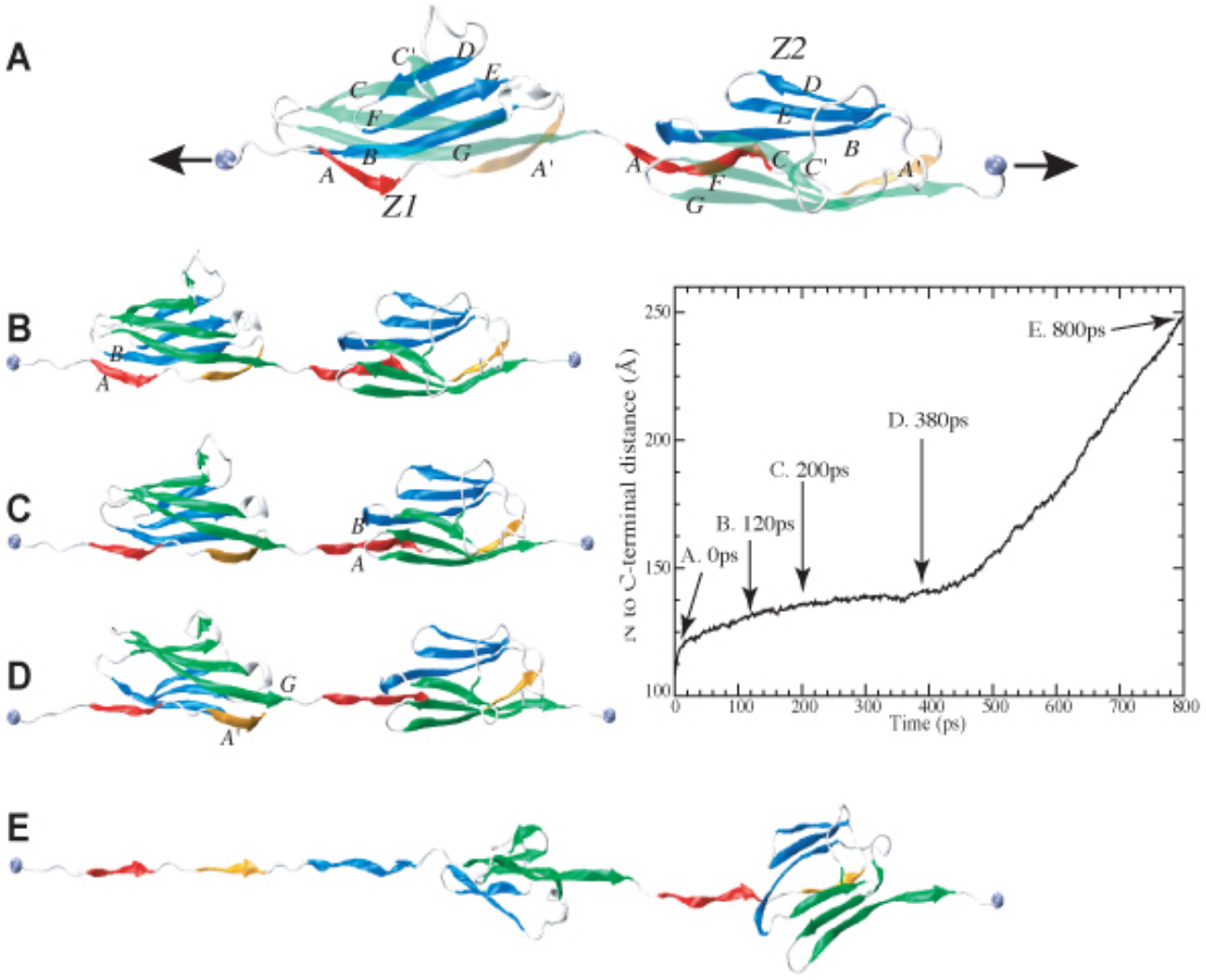
A
Z2
Z1
B
C
D
E
E. 800ps
D. 380ps
C. 200ps
B. 120ps
A. 0ps
N to C-terminal distance (Å)
Time (ps)

Figure 6:

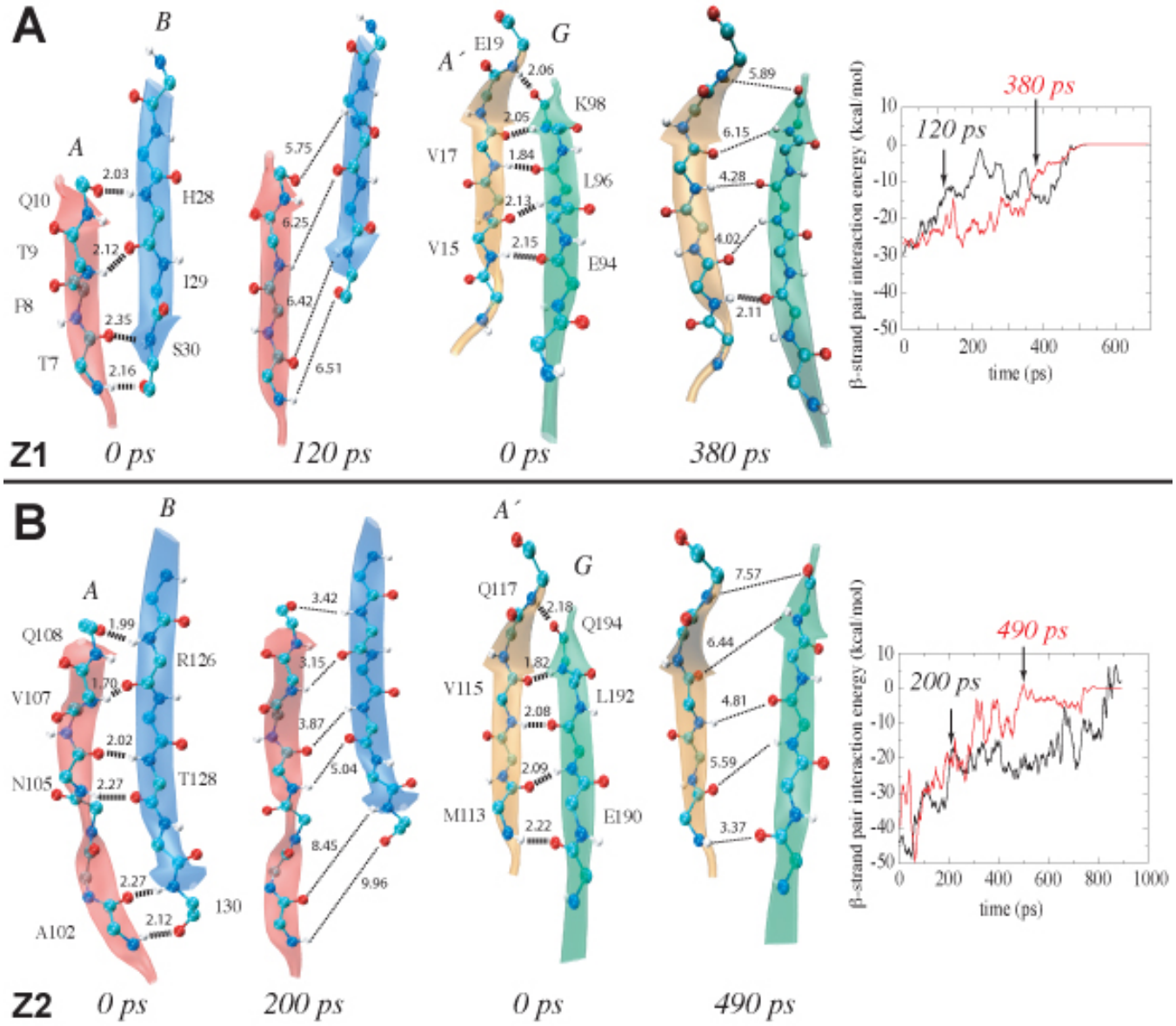
A
B
A
Q10
T9
F8
T7
H28
I29
S30
2.03
2.12
2.35
2.16
5.75
6.25
6.42
6.51
A´
E19
G
K98
V17
L96
V15
E94
2.06
2.05
1.84
2.13
2.15
5.89
6.15
4.28
4.02
2.11
380 ps
120 ps
β-strand pair interaction energy (kcal/mol)
time (ps)
Z1
0 ps
120 ps
0 ps
380 ps
B
B
A
Q108
V107
N105
A102
R126
T128
130
1.99
1.70
2.02
2.27
2.27
2.12
3.42
3.15
3.87
5.04
8.45
9.96
A´
G
Q117
Q194
V115
L192
M113
E190
2.18
1.82
2.08
2.09
2.22
7.57
6.44
4.81
5.59
3.37
490 ps
200 ps
β-strand pair interaction energy (kcal/mol)
time (ps)
Z2
0 ps
200 ps
0 ps
490 ps

Figure 7:

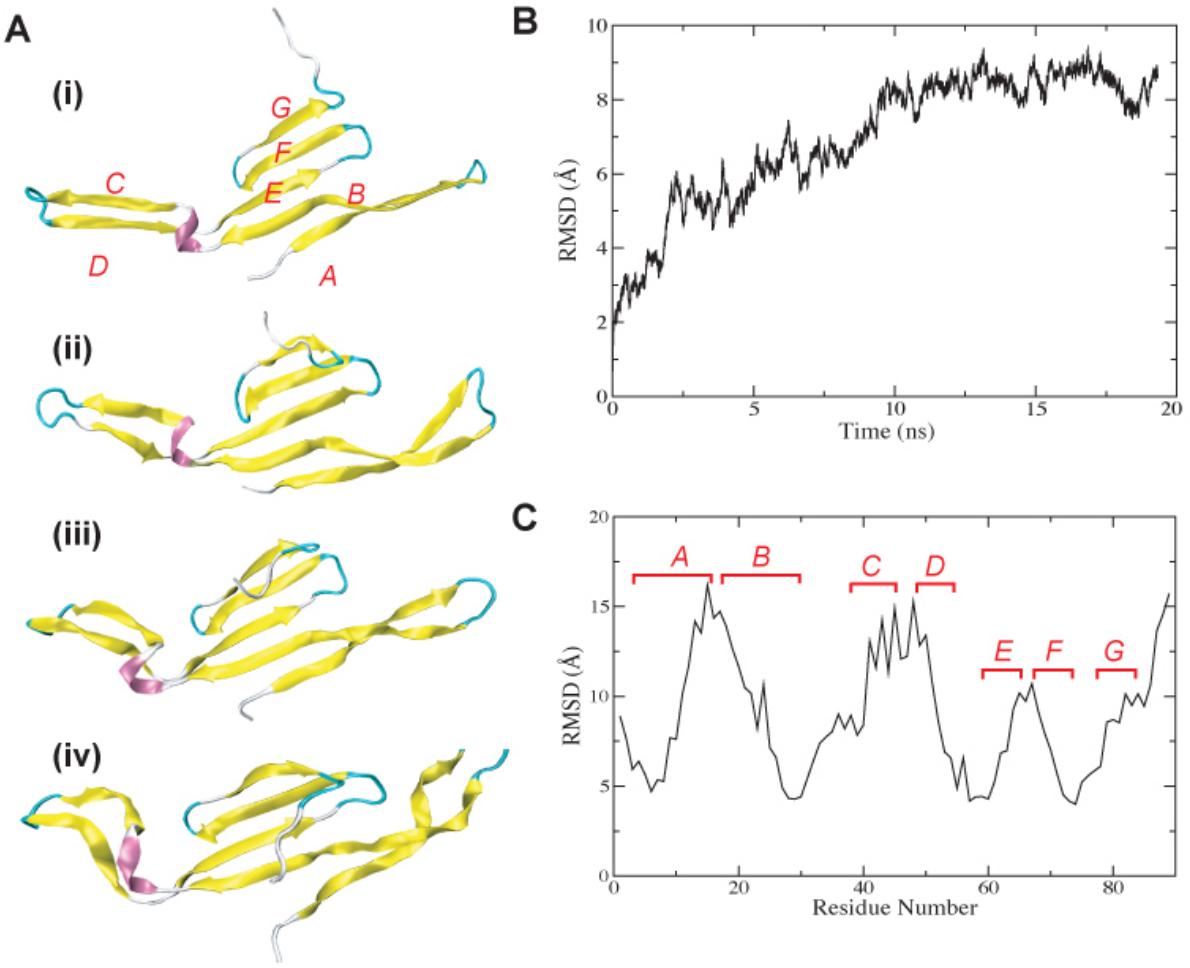
A
(i)
G
F
C
E
B
D
A
(ii)
(iii)
(iv)
B
RMSD (Å)
Time (ns)
C
A
B
C
D
E
F
G
RMSD (Å)
Residue Number

Figure 8: